Steel and Composite Structures, *Vol. 28, No. 1 (2018) 1-11*
DOI: https://doi.org/10.12989/scs.2018.28.1.001

Local ratcheting behavior in notched 1045 steel plates

K. Kolasangiani [1a], K. Farhangdoost [*1], M. Shariati [1b] and A. Varvani-Farahani [2b]

[1] *Department of Mechanical Engineering, Ferdowsi University of Mashhad, Azadi Square, Mashhad, Iran*
[2] *Department of Mechanical and Industrial Engineering, Ryerson University, Victoria Street, Toronto, Canada*

(*Received August 1, 2017, Revised January 21, 2018, Accepted April 10, 2018*)

Abstract. In this paper, local ratcheting behavior of 1045 steel plates with circular cutout was investigated. Experimental tests were carried out by a Zwick/Roell HB 100 servo hydraulic machine. In order to measure the local strain at notch root, a data acquisition system with strain gauge was used. Various notch diameters and distances of strain gauges mounted from the notch root were found influential in the magnitude of local ratcheting strain. It was found that the local maximum principal stress plays a crucial role in increasing the local plastic deformation. Numerical simulation was done by ABAQUS software using nonlinear isotropic/kinematic hardening model. Material parameters of hardening model were attained from several stabilized cycles of flat specimens subjected to symmetric strain cycles. The nonlinear kinematic hardening model along with the Neuber's rule was employed to assess local ratcheting at the notch root of steel plates. The results of the numerical simulations agreed closely with those measured values in this study. Both ratcheting progress and mean stress relaxation occurred simultaneously at the notch root.

Keywords: local ratcheting behavior; notch root; nonlinear isotropic/kinematic hardening model; Neuber's rule; 1045 steel plates

1. Introduction

Many engineering components contain notches like grooves, holes, etc. An existence of notches or geometrical discontinuities are necessary for mechanical connection in spite of the degradation of life imposed by them on the component. Moreover, components of structures are often exposed to cyclic loading. A cyclic accumulation of plastic deformation will occur in the components when a cyclic loading with nonzero mean force under force-control condition is applied. The plastic deformation in one cyclic loading may be low. However, its accumulation can be remarkable in one direction during loading. This phenomenon is called cyclic creep or ratcheting. It is important to consider the ratcheting in the design of structural components. In the last two decades, ratcheting and low cycle fatigue of materials have been extensively studied (Kang 2008, Kolasangiani and Shariati 2017, Shariati *et al*. 2012, 2016, Chen *et al*. 2015, 2016, Chen and Chen 2016, Huang *et al*. 2014, Lim *et al*. 2013, Ahmadzadeh and Varvani-Farahani 2012, Hamidinejad and Varvani-Farahani 2015, Ahmadzadeh and Varvani-Farahani 2016).

When a notched component is loaded, extensive plastic deformation appears at the notch root as a result of stress concentration. The local accumulated plastic strain in load-bearing components results in crack initiation and its growth around the notch accelerating failure. Therefore, design and analysis of structures with notches necessitate the study of cyclic behavior of notched specimens and the stress-strain at critical regions.

The local stress/strain of notched specimens undergoing cyclic loads has been studied extensively over the past several years (Sakane and Ohnami 1983, Sakane and Ohnami 1986, Fatemi *et al*. 2004, Varvani-Farahani *et al*. 2005, Medekshas and Balina 2006, Nozaki *et al*. 2011, Ince and Glinka 2013). Savaidis *et al*. (2001) studied the cyclic behavior of notched shaft by using an elastic-plastic finite element analysis. They observed that the local stress-strain behavior at the notch root was affected by the stress amplitude and the mean stress using the von-Mises yield criterion and the kinematic hardening rule of Prager/Ziegler. Wang and Rose (1998) studied the transient and steady-state cyclic behavior around the notch. They realized that both elastic-perfectly plastic and linear kinematic hardening models predict a quick plastic shakedown whereas the nonlinear kinematic hardening rule predicts a gradual shakedown while both ratcheting and mean stress relaxation occur simultaneously around the notch. Zeng and Fatemi (2001) studied the local stress-strain behavior of a vanadium-based microalloyed steel on the notched round bars and double-notched flat plates under the monotonic and cyclic loads.

Fatigue behavior of DZ125 solidified superalloy samples with single-edge notched was examined by Shi *et al*. (2013). They observed that the ratcheting is affected by both stress concentration factor and the applied nominal stress. They further indicated that the cracking occurs at the

*Corresponding author, Professor,
E-mail: Farhang@um.ac.ir
[a] Ph.D. Student,
E-mail: kamal.kolasangiani@mail.um.ac.ir
[b] Professor

ISSN: 1229-9367 (Print), 1598-6233 (Online)

Table 1 Chemical composition of AISI 1045 steel

Chemical composition	Fe	C	Mn	Si	Ni	S	P	Cr	Mo	Al	Cu	Co	N
%	98.3	0.445	0.56	0.261	0.085	0.005	0.017	0.123	0.006	0.02	0.142	0.004	0.007

Table 2 Mechanical properties of AISI 1045 steel from tensile test

Yield stress (MPa)	Modulus of elasticity (GPa)	Ultimate tensile stress (MPa)	Failure strain (%)
312	203	564	13

location where the maximum principal stress is the highest. Rahman and Hassan (2005) conducted cyclic and ratcheting tests on notched plates. Their experimental data were used to further improve ratcheting prediction by means of the Chaboche model.

The local ratcheting data at notch root have rarely been reported in the literature and the capability of the kinematic hardening rule in conjunction with the Neuber's rule to assess local ratcheting strain has not been studied broadly. The present study intends to examine local ratcheting of 1045 steel plates with circular cutout undergoing asymmetric loading cycles. Strain measurements were done by means of strain gauges mounted around the cutout. The material parameters of hardening model were obtained from experimental tests on flat 1045 steel specimens. Measured values of strains at notch root were compared with those determined through FE analysis by nonlinear isotropic/ kinematic hardening model. Both values of local strains from tests and numerical analysis were found in good agreements. Further, the measured values of strains at notch root through strain gauges agreed with those determined by means of the hardening rule as well as the Neuber's rule.

2. Experimental procedure

2.1 Materials, properties and test geometry

The material used in this study is AISI 1045 steel. The chemical composition of the material is given in Table 1. In order to determine the mechanical properties of AISI 1045, standard tension test was performed according to ASTME8. The result of mechanical properties is tabulated in Table 2.

2.2 Test device and boundary condition

Tests were conducted by a Zwick/Roell HB 100 servo hydraulic machine (Fig. 1(a)). The experimental tests were performed under load-control condition and the axial load was applied on the plates in the form of a sinusoidal wave (Fig. 1(b)).

Geometric dimensions and boundary conditions of the plates with circular cutout are shown in Fig. 1(b). The lower edge of the plate was clamped and the cyclic force was applied through a device jaw at the upper edge of the plate.

2.3 Local data acquisition

In order to analyze the local strain at the notch root, strain gauges and data acquisition system were used. The measurement system of the local strain during cyclic deformation was made using Wheatstone bridge circuit, amplifier and DAQ card (Fig. 2). This system was connected to a computer which acquired 100 data points per second. At any cycle of the test, local strain data as well as actuator displacements (global displacement) were continuously recorded. The strain gauge was used for the measurement of the local accumulated plastic strain.

3. Hardening model

The ratcheting response of materials was simulated with isotropic and kinematic hardening rules. It is generally not recommended to analyze the cyclic behavior of materials with isotropic hardening model since it always predicts shakedown during cyclic loading. So, it is better to use the

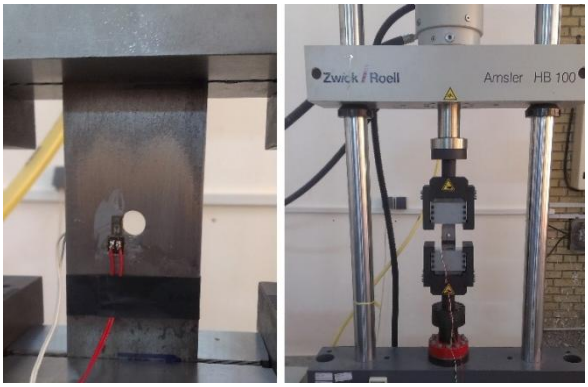

(a) Zwick/Roell HB 100 servo hydraulic machine

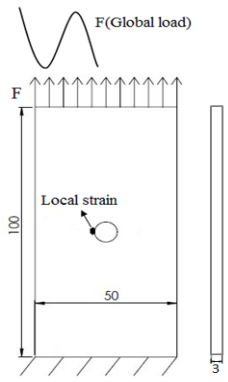

(b) Specimen geopmetry

Fig. 1 Experimental setup for testing of notched plates

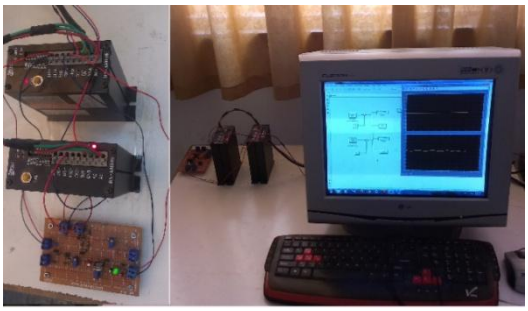

Fig. 2 Data acquisition system

kinematic hardening model or the (combined) nonlinear isotropic/kinematic hardening model to simulate the cyclic behavior of materials. The nonlinear isotropic/ kinematic hardening model has two components: a nonlinear kinematic hardening component and an isotropic hardening component.

3.1 Isotropic hardening model

The isotropic hardening model states that the yield surface size changes uniformly in all directions during the plastic deformation. Assuming isothermal plastic deformation, time independent plasticity, and by using von-Mises criterion the yield surface can be written in the form of (Chaboche 1989)

$$f = J_2(\sigma) - R - k \tag{1}$$

where k is the uniaxial yield stress, R is the isotropic hardening parameter which is a function of the equivalent plastic strain p and J_2 is the von-Mises distance in the deviatoric stress space (Chaboche 1989). The equivalent plastic strain rate dp is also defined as

$$dp = \sqrt{\frac{2}{3} d\varepsilon^p : d\varepsilon^p} \tag{2}$$

where $d\varepsilon^p$ is the rate of plastic strain.

The isotropic hardening rule can be utilized as an independent hardening mechanism regardless of the kinematic hardening rule. For isothermal plastic deformation, Chaboche (1989) suggested the isotropic hardening as

$$dR = b(Q - R)dp \tag{3}$$

where Q and b are two material constants. This equation states that irrespective of the kinematic hardening rule and the loading condition, the parameter R varies as a function of the accumulated equivalent plastic strain p. By integrating the above equation with the initial value $R = 0$ and considering Eq. (1), the instantaneous yield surface size is determined as

$$\sigma^0 = k + Q(1 - exp(-bp)) \tag{4}$$

3.2 Nonlinear kinematic hardening model

The kinematic hardening model may be chosen to simulate the cyclic behavior of materials. The kinematic hardening model describes that the subsequent yield surfaces move without changing its size in the stress space under the plastic deformation. Armstrong and Frederick (1966) proposed the first nonlinear kinematic hardening model.

The yield surface which is based on the von-Mises yield criterion, for time independent plasticity is defined as (Lemaitre and Chaboche 1994)

$$f(\sigma - X, k) = \sqrt{\frac{3}{2}(\sigma' - X') : (\sigma' - X')} - k \tag{5}$$

where σ and X are the stress tensor and backstress tensor, respectively. σ' is the deviatoric stress tensor, X' is the deviatoric backstress tensor indicating the center of the yield surface and k is the initial size of the yield surface. Armstrong and Frederick (A-F) proposed a nonlinear kinematic hardening rule in the form of

$$dX = \frac{2}{3} C d\varepsilon^p - \gamma X dp \tag{6}$$

where C and γ are material constants. Equations (7-9) were defined by Lemaitre and Chaboche (1994) through the A-F model under uniaxial loading condition as

$$f = |\sigma - X| - k = 0 \tag{7}$$

$$dX = C d\varepsilon^p - \gamma X |d\varepsilon^p| \tag{8}$$

The solution of Eq. (8) is defined as

$$\begin{aligned} X &= \frac{C}{\gamma} + \left(X_0 - \frac{C}{\gamma}\right) exp\left[-\gamma\left(\varepsilon^p - \varepsilon_0^p\right)\right], \quad d\varepsilon^p \geq 0 \\ X &= -\frac{C}{\gamma} + \left(X_0 + \frac{C}{\gamma}\right) exp\left[\gamma(\varepsilon^p - \varepsilon_0^p)\right], \quad d\varepsilon^p < 0 \end{aligned} \tag{9}$$

where X_0 is the initial backstress and ε_0^p is the initial plastic strain.

It should be mentioned that the Eq. (7) applies to stabilized cycles as well as transient ones. In a stable cycle, the maximum and minimum stress and strain are constant during a cycle. Furthermore, the plastic strain at the end of one excursion (the loading branch) will be the initial value for the next one (the unloading and reloading branch). Through definition of plastic strain range ($\Delta\varepsilon^p = \varepsilon^p_{\max} - \varepsilon^p_{\min}$), the stress range as ($\Delta\sigma = \sigma_{\max} - \sigma_{\min}$), and their substitution into Eqs. (7)-(9), the relation between the half stress range and half strain range under stabilized cycling is expressed as

$$\frac{\Delta\sigma}{2} - k = \frac{C}{\gamma} \tanh\left(\gamma \frac{\Delta\varepsilon^p}{2}\right) \tag{10}$$

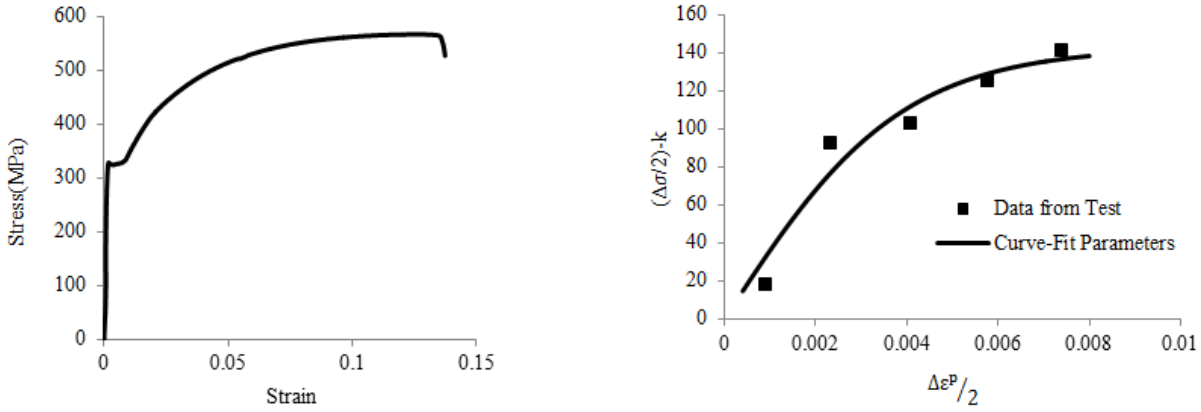

(a) Stress-strain curve of tension test (b) Curve-fit data

Fig. 3 Results of combined isotropic/kinematic hardening model

3.3 Nonlinear isotropic/kinematic (combined) hardening model

The von-Mises yield criterion, the associated flow rule and the isotropic and kinematic strain hardening are the main elements of the combined hardening rule.

It is important to accurately determine the hardening model parameters. In order to attain combined hardening parameters correctly, the hardening model could be calibrated by experimental data. The calibration procedure consists of six plate specimens, one of which was subjected to tensile load up to necking point to obtain the isotropic hardening components and others (five specimens) were put under symmetric strain-control condition with different strain amplitudes. Three different methods are usually used to determine the kinematic hardening parameters. Three types of data are obtained from experimental tests: (i) data of half-cycle; (ii) data of single stabilized cycle; (iii) data of several stabilized cycles (Azadeh and Taheri 2015). In the current research, the third approach is used to determine the kinematic hardening parameters of specimens which are subjected to cyclic symmetric strain loading.

The kinematic hardening parameters, C and γ could be obtained by fitting Eq. (10) to the experimental data from stabilized cycles in Fig. 3(b).

Under symmetric strain-control loading, by summing the absolute value of the change in axial plastic strains, the equivalent plastic strain $\bar{p}$ is defined using (Azadeh and Taheri 2015)

$$\bar{p} = \sum_i \left| \Delta\varepsilon_i - {}^{\Delta\sigma_{exp}}/_{E} \right| \qquad (111)$$

where ε_i is the total strain, $\sigma_{\exp}$ is the applied stress in during a test and E is the Young's modulus.

The equivalent stress corresponding to the equivalent strain was determined by an empirical equation through regression of data collected over tensile test. The monotonic hardening curve (Eq. (12)) is fit to the experimental data with strains ranging from half of the necking strain up to the necking strain in Fig. 3(a), using nonlinear least-squares regression (Azadeh and Taheri 2015)

$$\bar{\sigma} = \sigma_y \left(1 + \frac{\bar{p}}{m}\right)^n \qquad (12)$$

In Eq. (12), $\bar{\sigma}$ is the equivalent stress and σ_y is the initial axial yield stress. Also, m and n are material constants. The equivalent backstress $\bar{X}$ and the equivalent stress $\bar{\sigma}$ were obtained at any increment of the equivalent plastic strain by fitting Eqs. (9)-(12) to the experimental data, respectively. According to Eq. (13), the instantaneous yield surface size σ^0 is defined as a discrepancy between the equivalent stress and the equivalent backstress

$$\sigma^0(\bar{p}) = \bar{\sigma}(\bar{p}) - \bar{X}(\bar{p}) \qquad (13)$$

The isotropic hardening material parameters, Q and b, could be determined when the Eq. (4) is fit to the results obtained by Eq. (13) by using the nonlinear least-squares regression method.

The kinematic and isotropic hardening parameters were determined as $C = 36692$ MPa , $\gamma = 193.5$, $Q = 217.5$ MPa, $b = 3.48$.

ABAQUS software was used to simulate the ratcheting behavior of the plate numerically. The same boundary conditions as earlier defined for ratcheting tests were employed. The testing plate was sandwiched between two rigid plates at its both ends (upper and lower ends). Lower rigid plate was constrained in all translational and rotational directions (U1 = U2 = U3 = UR1 = UR2 = UR3 = 0). The upper rigid plate was constrained in the same way in all directions except the direction of the loading (U3). Then the upper rigid plate was subjected to cyclic loading under force-controlled condition.

Element S8R5 was used in numerical simulation. It is an eight node shell element with five degree of freedom in each node. Due to the stress concentration around the notch, the sizes of the elements in the vicinity of the notch are smaller. Fig. 4 presents a portion of meshed plate.

4. Experimental results

In order to be succinct in this research, "force" and

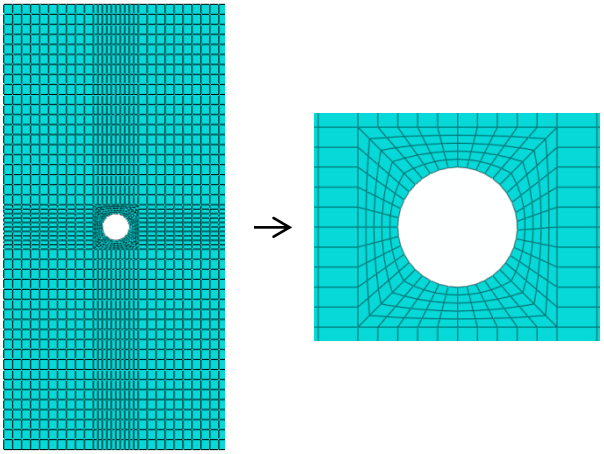

Fig. 4 Meshed notched sample

"displacement" are employed rather than "global force" and "global displacement" respectively. All tests were performed in the force-control condition with non-zero mean force.

The ratcheting displacement is the maximum global displacement determined over each cycle. The local ratcheting strain will be defined as the average of maximum and minimum local strain in each cycle.

4.1 Effect of notch diameter

In order to investigate the effect of notch diameter on the local ratcheting behavior, some experimental tests were carried out on the plates with notch diameter of 3, 6, 7, 8 and 9 mm. To measure the local strain at the notch root, strain gauges were arranged at distances X = 0.5, 1.5 and 2.5 mm from the notch root as shown in Fig. 7(a). The global and local plastic deformation versus the number of cycles under asymmetrical loading cycles of 25 kN ± 25 kN are presented in Figs. 5(a)-(b). This non-zero mean force leads to a non-zero local mean stress which subsequently results in global and local ratcheting. It is observed that with increasing the notch diameter, the ratcheting displacement and the local ratcheting strain for a certain cycle increases.

The total accumulation of plastic deformation can be divided into two parts, a local part around the notch and nominal part far away from the notch. Since the geometric dimensions of the plates are similar, the nominal part is equal for all specimens under the identical loading. The local part, which is controlled by maximum principal stress, is the main parameter for increasing the global and local plastic deformation. Therefore, based on the experimental results and comparing the local and global ratcheting strains in Figs. 5(a)-(b), it can be concluded that the global

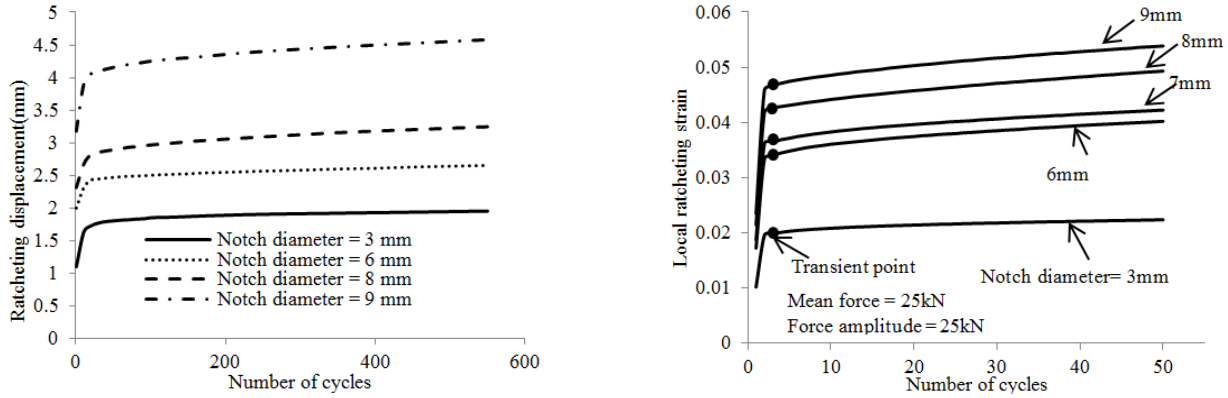

(a) Nominal ratcheting displacement (b) Local ratcheting strain

Fig. 5 Ratcheting strain over stress cycles for various notch diameters

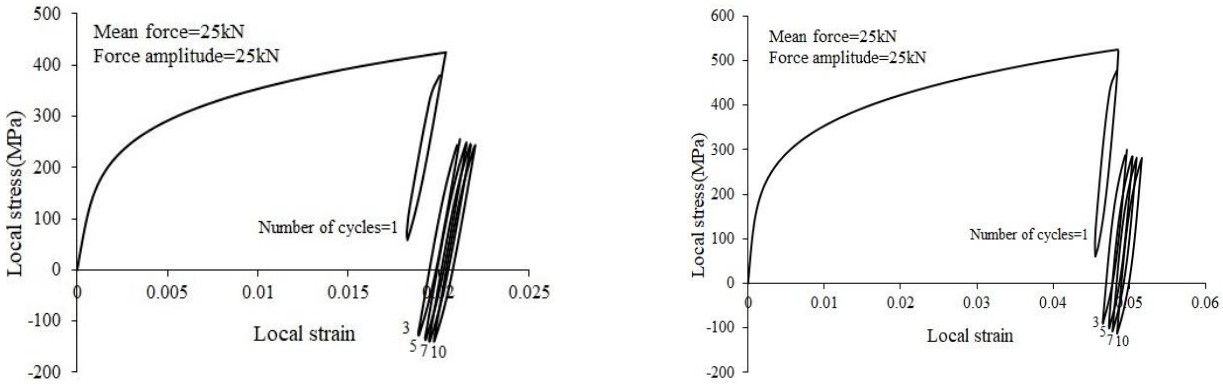

(a) Notch diameter = 3 mm (b) Notch diameter = 9 mm

Fig. 6 Generated stress-strain hysteresis loops over local ratcheting progress at the notch root vicinity

ratcheting is governed by the local strain. Also the maximum principal stress around the notch root can be a main control factor that influences the local and global plastic deformation and life of the notched specimens (Shi *et al*. 2013).

For each sample, with raising the number of cycles, the local and global ratcheting increase while their rates decrease until the ratcheting rate almost becomes constant. The decrease in the ratcheting rate and its inclination toward zero, or in other words, the cessation of plastic deformation accumulation (ratcheting) is due to the formation and the extent of dislocations with cyclic loading. When a substance is under cyclic loading, dislocations in its structure are created by strain hardening. These dislocations were initially placed in a chaotic state, then as the number of cycles goes up, they turn into the elements of orderly dislocation (Dutta and Ray 2012).

According to Fig. 5(b), there is a transient point demarcating the region with a high local ratcheting strain rate and the region with constant local ratcheting strain rate (Shariati *et al*. 2014). It is observed that as the notch diameter increases, the transient point occurs in higher local ratcheting strain.

Figs. 6(a)-(b) shows the hysteresis loops generated at the notch root vicinity for cycles 1, 3, 5, 7, and 10 at distance X = 0.5 mm from the notch root for notch sizes d = 3, 9 mm under the cyclic loading 25 kN ± 25 kN. Mean stress relaxation at the notch root was evidenced along with ratcheting progress as hysteresis loops shifted to lower stresses over loading cycles.

4.2 Effect of strain gauge position around the notch root

The strain gauges were arranged on different distances X = 0.5, 1.5, 2.5 mm along the horizontal centerline from the notch root (Fig. 7(a)). Plates with 9 mm notch diameter were subjected to cyclic loading with the force amplitude and mean force of 25 kN ± 25 kN. Fig. 7(b) shows the local ratcheting strain based over stress cycles for an un-notched plate and three notched plates with the strain gauges mounted at 0.5, 1.5 and 2.5 mm distances from the notch root. Fig. 7(b) verifies how noticeable is the ratcheting of notched plates as compared with the un-notched one. This behavior results from the rise of maximum stress, which is caused by the presence of the stress concentration around the notch root. It was also observed that as the strain gauge are positioned farther away from the notch root, the measured local ratcheting strain is reduced. The largest stress occurs around the notch root which leads to different ratcheting strains in different locations around the notch.

5. Numerical results

Finite element method was employed to assess local ratcheting at the notch roots. The combined isotropic/ kinematic hardening rule along the Neuber's rule was utilized to simulate the local ratcheting behavior of the notched plates.

5.1 Influence of mean force and force amplitude

To analyze the influence of mean force and force amplitude on the local ratcheting behavior, a number of plates with 8 mm notch diameter were subjected to cyclic axial loading. Fig. 8(a) shows the local ratcheting strain versus the number of cycles for three plates with loading cycles 25 kN ± 25 kN, 26 kN ± 25 kN, 27 kN ± 25 kN. It is observed that as the mean force increases, the local ratcheting strain and its rate increases for a number stress cycle. Under force-control loading with constant force amplitude, raising of mean force, leads to raise of local maximum principal stress and finally higher plastic deformation around the notch root.

In addition, Fig. 8(b) presents the local ratcheting strain versus the number of cycles for various loading conditions of 30 kN ± 25 kN, 30 kN ± 26 kN, and 30 kN ± 27 kN. An increase of force amplitude resulted in maximum principal stress and local accumulated plastic strain at the notch root. The local ratcheting strain and the local plastic strain at the transient point increased mainly due to the fact that the maximum principal stress increased locally in above loading cases. This phenomenon is related to the dislocation density of the substructure under the cyclic loading. Some dislocations remain as residual in the substructure of the

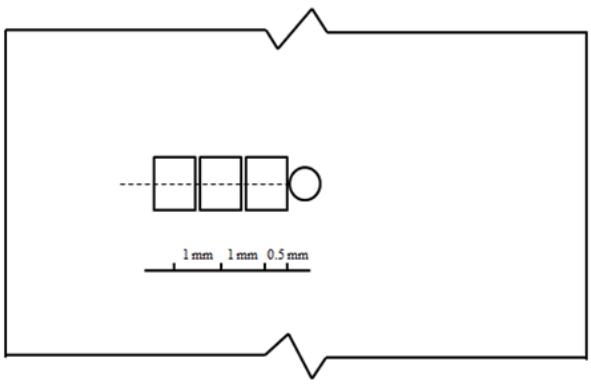

(a) Different strain gauge arrangements around the notch

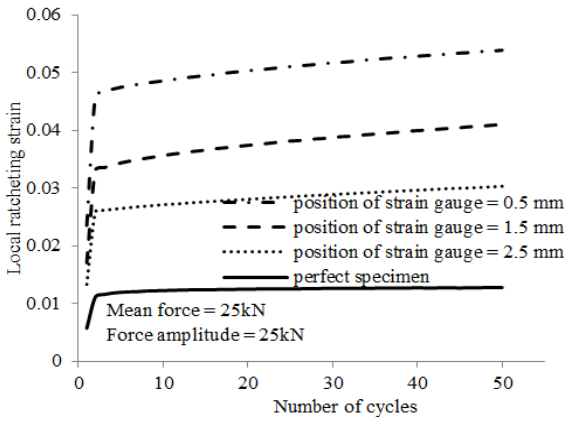

(b) Local ratcheting strain curves

Fig. 7 Positions of strain gauges around the notch and corresponding ratcheting response over loading cycles

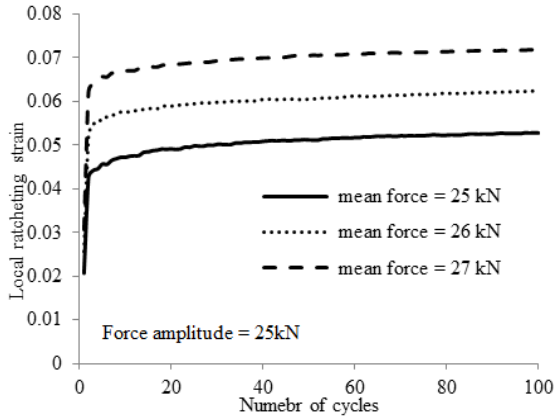

(a) Effect of mean force on local ratcheting strain

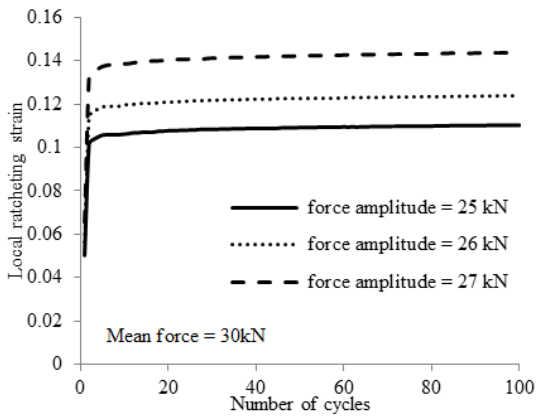

(b) Effect of force amplitude on local ratcheting strain

Fig. 8 Local ratcheting strain versus the number of cycles for different applied forces

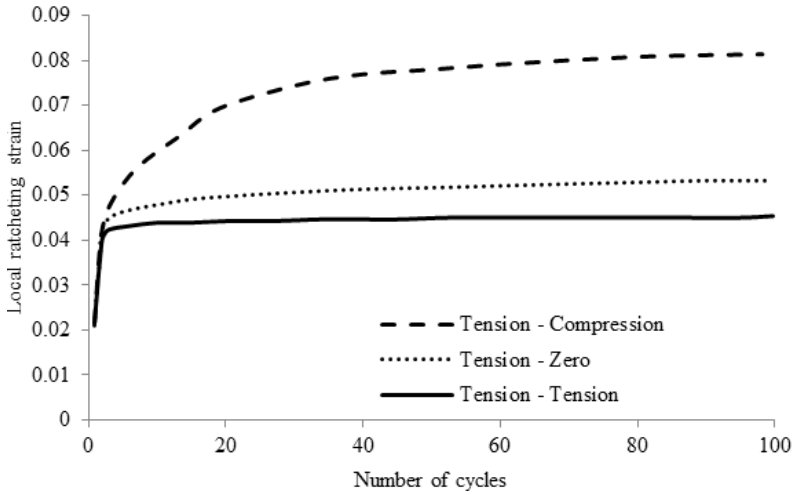

Fig. 9 Influence of load regime on the local ratcheting strain of the notched plate

Table 3 Influence of load regime on the local ratcheting strain and number of cycles at transient point

Loading regime	Nominal mean force (kN)	Nominal force amplitude (kN)	$R = \frac{F_{\min}}{F_{\max}}$	Local ratcheting strain at transient point	Number of cycles at transient point
Tension - Tension	30	20	0.2	0.0431	6
Tension - Zero	25	25	0	0.0491	15
Tension - Compression	20	30	-0.2	0.0768	39

material at the notch root and as the maximum principal stress increases, the residual dislocation density is magnified locally.

5.2 Effect of cyclic load regime

Three plates with 8 mm notch diameter were subjected to cyclic loading. The three load regimes were defined as (i) tension-tension; (ii) tension-zero; (iii) tension-compression. The prescribed loading conditions and details of the transient point for each load regime are given in Table 3. The peak tension force during three load cases was constant (i.e., 50 kN). Fig. 9 depicts the local ratcheting strain versus the number of cycles. It is observed that by changing the load case from tension-tension to tension-zero and then to tension-compression cases, the local ratcheting strain and its rate increase noticeably. According to Table 3 and Fig. 9, it is found that the transient point occurs in higher local ratcheting strain and at a later time as the load regime changes from tension-tension to tension-compression conditions. In other words, the cyclic load with tension-tension regime causes the accumulation of local plastic deformation to reach a constant rate faster.

5.3 Effect of hardening parameters

In order to investigate the sensitivity of the local ratcheting behavior to the hardening model, the influence of

Table 4 Effect of material hardening parameters on the local ratcheting strain and number of cycles at transient point

Model number	Loading mean ± amplitude	C (MPa)	γ	Q (MPa)	b	Local ratcheting strain at transient point	Number of cycles at transient point
1	20 kN ± 30 kN	36692	193.5	217.5	3.48	0.0768	39
2	20 kN ± 30 kN	35591	193.5	217.5	3.48	0.0813	34
3	20 kN ± 30 kN	37792	193.5	217.5	3.48	0.0736	53
4	20 kN ± 30 kN	36692	187.6	217.5	3.48	0.074	45
5	20 kN ± 30 kN	36692	199.3	217.5	3.48	0.0806	29
6	20 kN ± 30 kN	36692	193.5	210.9	3.48	0.0791	33
7	20 kN ± 30 kN	36692	193.5	224	3.48	0.0743	42
8	20 kN ± 30 kN	36692	193.5	217.5	3.37	0.0788	38
9	20 kN ± 30 kN	36692	193.5	217.5	3.58	0.0752	41

the hardening parameters was studied for a plate with 8 mm notch diameter. For loading case 20 kN ± 30 kN applied on the plate in the compression-tension, the kinematic and isotropic hardening parameters were changed by approximately 3% with respect to the first model in previous sections (See Table 4). This table evaluates the sensitivity of the hardening parameters and its influence on the local ratcheting response. The transient point is assumed as a criteria for comparing the ratcheting behavior of different hardening parameters. The local ratcheting strain and number of cycles at transient points are reported in the table. A drop in the values of C, Q and an increase in γ, the transient point occurs in fewer number of cycles while the local ratcheting strain at this point increases.

Thus, in order to accurately simulate the local ratcheting behavior of notched plate, it is necessary to choose a correct hardening parameter. The results indicate that the local ratcheting behavior shows lower sensitivity to a change in

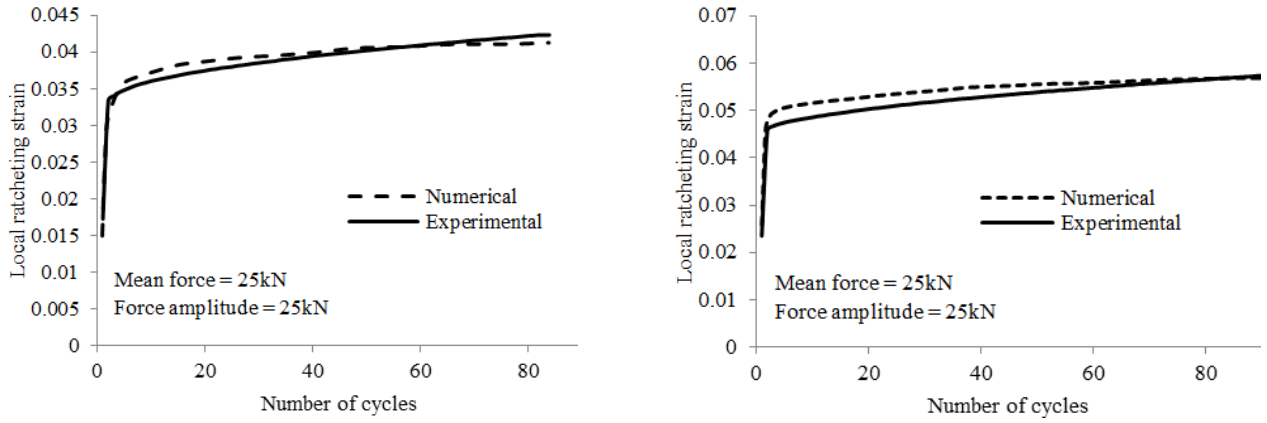

(a) Notch diameter = 6 mm (b) Notch diameter = 9 mm

Fig. 10 Experimental and numerical ratcheting strain data for the notched plates

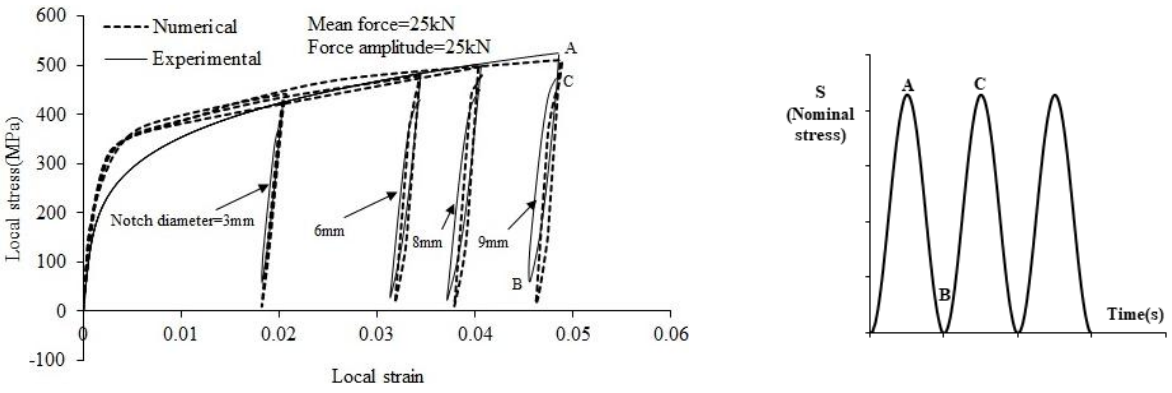

Fig. 11 Experimental and numerical hysteresis loops generated at the notch root of various notch sizes

term b.

6. Confirmation of numerical results with experimental findings

The local ratcheting results obtained through measurements and numerical simulations on notched plates for loading case 25 kN ± 25 kN are shown in Figs. 10-11. In Fig. 10, it is seen that the local ratcheting strain increases, whereas its rate reduces continuously with an increase in number of cycles. The measured data in this figure show more plastic strain accumulation rate as compared with those of numerical data. When the nonlinear isotropic/ kinematic hardening model is applied, a gradual plastic shakedown occurs around the notch root and the existence of the ratcheting is due to the fact that plastic yielding is no longer localized to the notch root area (Wang and Rose 1998). The local ratcheting results evaluated by numerical analysis were found in good agreement with those obtained experimentally.

The combined hardening rule enabled to further assess hysteresis loops generated at notch root over asymmetric cycles for various notch sizes. Fig. 11 compares hysteresis loops generated over the first cycle for notch sizes 3, 6, 8, and 9 mm through numerical and measured values. Good agreements between generated loops and experimentally obtained loops were achieved. As the notch diameter increased, the local mean stress increased for both numerical and experimental results in this figure.

7. The Neuber's rule for estimating of local accumulated strain

In order to determine the local ratcheting behavior of notched plate under asymmetric loading cycles, given the case of plane stress and assumption of uniaxial loading, the von-Mises yield criteria (Eq. (5)) and nonlinear kinematic hardening rule (Eq. (6)) can be written into the forms as Eqs. (7)-(8) respectively. Based on this assumption from Eq. (7), the relation between stress and backstress can be expressed as

$$\begin{aligned} X &= \sigma - k \qquad d\varepsilon^P \geq 0 \\ X &= \sigma + k \qquad d\varepsilon^P < 0 \end{aligned} \tag{14}$$

For the global stress with the non-zero mean stress (as sketched in Fig. 11), by combining Eqs. (9)-(14), the strain ranges for unloading path (e.g., AB in Fig. 11) and reloading path (e.g., BC in Fig. 11) are calculated through Eq. (15) (Wang and Rose 1998)

$$\begin{aligned} \varepsilon_B - \varepsilon_A &= \frac{\sigma_B - \sigma_A}{E} + \frac{1}{\gamma} ln \frac{\left(\sigma_B + \sigma_0 + \frac{C}{\gamma}\right)}{\left(\sigma_A - \sigma_0 + \frac{C}{\gamma}\right)} \qquad d\varepsilon^P < 0 \\ \varepsilon_C - \varepsilon_B &= \frac{\sigma_C - \sigma_B}{E} - \frac{1}{\gamma} ln \frac{\left(\sigma_C - \sigma_0 - \frac{C}{\gamma}\right)}{\left(\sigma_B + \sigma_0 - \frac{C}{\gamma}\right)} \qquad d\varepsilon^P \geq 0 \end{aligned} \tag{15}$$

In 1968, Neuber's rule was proposed for a notched body under pure shear, tension and bending loads (Neuber 1968). By using the Neuber's rule, the global stress and strain correlate with local stress and strain. In each half cycle, for globally elastic behavior, based on the Neuber's rule, the notch root stress and strain ranges can be related to global stress increment Δs using Hooke's law as

$$(\varepsilon_C - \varepsilon_B)(\sigma_C - \sigma_B) = \frac{(K_t(S_C - S_B))^2}{E} \tag{16}$$

where K_t is the stress concentration factor. The local stress and strain in each reversal point by using Eqs. (15)-(16) are determined for loading and unloading paths.

To verify the above method, some experimental tests were carried out on notched plates. The stress concentration factor (K_t) of notch diameter 6, 9, 12 and 15 mm are 2.64, 2.53, 2.43 and 2.36 respectively. The notched plates were subjected to cyclic loading of 16 kN ± 16 kN. Eq. (16) is employed as the maximum global stress 213.34 MPa is lower than the tensile yield strength. Fig. 12 compares the prediction of the Neuber's rule with experimental values. It is shown that the Neuber's rule overpredict the maximum local strain for the initial cycles in the bceginning of loading

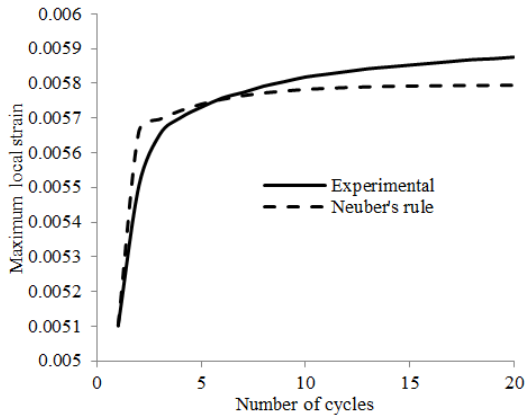

(a) Notch diameter = 9 mm

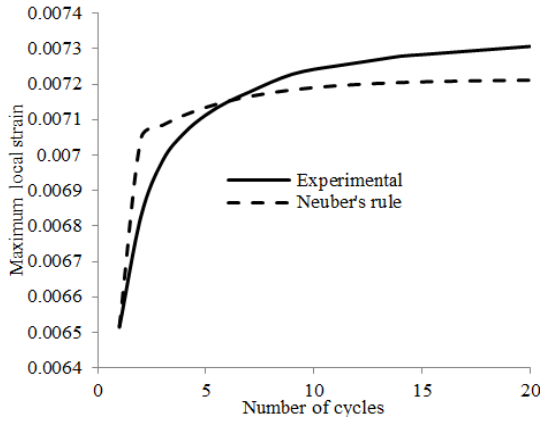

(b) Notch diameter = 12 mm

Fig. 12 Experimental and predicted Maximum local strain from the Neuber's rule for the notched plate

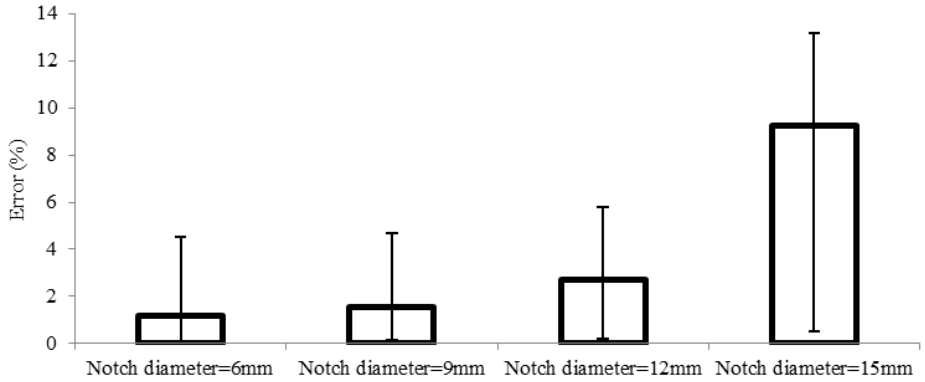

Fig. 13 Mean error for maximum local strain prediction using the Neuber's rule with respect to experimental results for different notch diameter

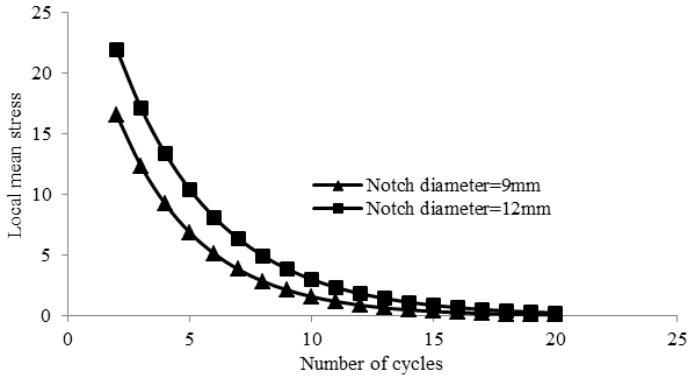

Fig. 9 Influence of load regime on the local ratcheting strain of the notched plate

but after the first cycle, the rate of local accumulated strain from the Neuber's rule is lower than the experimental results. When the A-F hardening model is used, a gradual plastic shakedown occurs at the notch root, as shown in Figs. 12(a)-(b). However, according to Fig. 12, the prediction of the Neuber's rule for estimating the local ratcheting strain is acceptable. Fig. 13 plots the mean error and error bar as a function of notch diameter for 20 cycles. The mean error increases with decreasing the stress concentration factor (K_t). As the notch diameter increases (K_t decreases), the plasticity spreads at a larger area. The accuracy of the Neuber's rule is lower for larger plastic zone at the notch root because of transition from localized plasticity to large scale yielding (Wang and Rose 1998).

Fig. 14 presents the results of mean stress relaxation for two notch sizes of 9 and 15 mm. The mean stress reduction is rapid over the initial loading cycles, but the rate of mean stress reduction decreases, rapidly as the number of cycles increases. Both stress concentration and ratcheting progress occur at notch root, simultaneously. Due to intense dependency of ratcheting on mean stress, it can be concluded that eventually the accumulation of local plastic strain will come to a stop, as the local mean stress gradually relaxes.

8. Conclusions

The present paper intended to evaluate local ratcheting behavior of 1045 steel plates at the notch root. A method was proposed to predict the local stress and strain using the Neuber's rule along with combined hardening rule. Various notch diameters and distances of strain gauges mounted from the notch root were found influential in the magnitude of local ratcheting strain. It was found that the local maximum principal stress highly influences the local plastic deformation. Numerical simulation results through ABAQUS software employing nonlinear isotropic/ kinematic (combined) hardening model were found in good agreement with those of measured data. The nonlinear kinematic hardening model along with the Neuber's rule were employed to assess local ratcheting at the notch root of steel plates. Both ratcheting progress and mean stress relaxation occurred simultaneously at the notch root

References

Ahmadzadeh, G.R. and Varvani-Farahani, A. (2012), "Concurrent ratcheting–fatigue damage analysis of uniaxially loaded A-516 Gr.70 and 42CrMo Steels", *Fatigue Fract. Eng. Mater. Struct.*, **35**, 962-970.

Ahmadzadeh, G.R. and Varvani-Farahani, A. (2016), "A kinematic hardening rule to investigate the impact of loading path and direction on ratcheting response of steel alloys", *Mech. Mater.*, **101**, 40-49.

Armstrong, P.J. and Frederick, C.O. (1966), "A mathematical representation of the multiaxial Bauschinger effect", Report RD/B/N731, CEGB, Central Electricity Generating Board,

Berkeley, CA, USA.
Azadeh, M. and Taheri, F. (2015), "Computational simulation of ratcheting in dented pipes due to monotonic and cyclic axial loading", *J. Strain. Anal. Eng.*, **50**(3), 163-174.
Chaboche, J.L. (1989), "Constitutive equations for cyclic plasticity and cyclic viscoplasticity", *Int. J. Plast.*, **5**(3), 247-302.
Chen, X. and Chen, X. (2016), "Effect of local wall thinning on ratcheting behavior of pressurized 90° elbow pipe under reversed bending using finite element analysis", *Steel Compos. Struct., Int. J.*, **20**(4), 931-950.
Chen, X., Chen, X., Chen, G. and Li, D. (2015), "Ratcheting behavior of pressurized Z2CND18.12N stainless steel pipe under different control modes", *Steel Compos. Struct., Int. J.*, **18**(1), 29-50.
Chen, X., Gao, B. and Chen, X. (2016), "Evaluation of AF type cyclic plasticity models in ratcheting simulation of pressurized elbow pipes under reversed bending", *Steel Compos. Struct., Int. J.*, **21**(4), 703-753.
Dutta, K. and Ray, K. (2012), "Ratcheting phenomenon and post-ratcheting tensile behaviour of an aluminum alloy", *Mater. Sci. Eng.*, **540**, 30-37.
Fatemi, A., Zeng, Z. and Plaseied, A. (2004), "Fatigue behavior and life predictions of notched specimens made of QT and forged microalloyed steels", *Int. J. Fatigue*, **26**(6), 663-672.
Hamidinejad, S.M. and Varvani-Farahani, A. (2015), "Ratcheting assessment of steel samples under various non-proportional loading paths by means of kinematic hardening rules", *Mater. Des.*, **85**, 367-376.
Huang, Z., Wang, Q., Wagner, D. and Bathias, C. (2014), "Constitutive model coupled with damage for carbon manganese steel in low cycle fatigue", *Steel Compos. Struct., Int. J.*, **17**(2), 185-198.
Ince, C. and Glinka, G. (2013), "A numerical method for elasto-plastic notch-root stress–strain analysis", *J. Strain. Anal. Eng.*, **48**(4), 229-244.
Kang, G. (2008), "Ratchetting: recent progresses in phenomenon observation, constitutive modeling and application", *Int. J. Fatigue*, **30**(8), 1448-1472.
Kolasangiani, K. and Shariati, M. (2017), "Experimental study of SS304L cylindrical shell with/without cutout under cyclic combined and uniaxial loading", *Int. J. Steel Struct.*, **17**(2), 553-563.
Lemaitre, J. and Chaboche, J.L. (1994), *Mechanics of Solid Materials*, Cambridge University Press, London, England.
Lim, C., Choi, W. and Sumner, E.A. (2013), "Parametric study using finite element simulation for low cycle fatigue behavior of end plate moment connection", *Steel Compos. Struct., Int. J.*, **14**(1), 57-71.
Medekshas, H. and Balina, V. (2006), "Assessment of low cycle fatigue strength of notched components", *Mater. Des.*, **27**(2), 132-140.
Neuber, H. (1968), "A physically nonlinear notch and crack model", *J. Mech. Phys. Solids*, **16**, 289-294.
Nozaki, M., Zhang, S., Sakane, M. and Kobayashi, K. (2011), "Notch effect on creep–fatigue life for Sn–3.5 Ag solder", *Eng. Fract. Mech.*, **78**(8), 1794-1807.
Rahman, S.M. and Hassan, T. (2005), "Advanced Cyclic Plasticity Models in Simulating Ratcheting Responses of Straight and Elbow Piping Components, and Notched Plates", *Proceedings of PVP-2005*, Denver, USA, July.
Sakane, M. and Ohnami, M. (1983), "A study on the notch effect on the low cycle fatigue of metals in creep-fatigue interacting conditions at elevated temperature", *J. Eng. Mater. Technol.*, **105**(2), 75-80.
Sakane, M. and Ohnami, M. (1986), "Notch Effect in Low-Cycle Fatigue at Elevated Temperatures—Life Prediction From Crack Initiation and Propagation Considerations", *J. Eng. Mater. Technol.*, **108**(4), 279-284.
Savaidis, A., Savaidis, G. and Zhang, C. (2001), "Elastic–plastic FE analysis of a notched shaft under multiaxial nonproportional synchronous cyclic loading", *Theor. Appl. Fract. Mech.*, **36**(2), 87-97.
Shariati, M., Hatami, H., Torabi, H. and Epakchi, H. (2012), "Experimental and numerical investigations on the ratcheting characteristics of cylindrical shell under cyclic axial loading", *Struct. Eng. Mech., Int. J.*, **44**(6), 753-762.
Shariati, M., Kolasangiani, K., Norouzi, G. and Shahnavaz, A. (2014), "Experimental study of SS316L cantilevered cylindrical shells under cyclic bending load", *Thin-Wall. Struct.*, **82**, 124-131.
Shariati, M., Kolasangiani, K. and Golmakani, H. (2016), "Cyclic behavr of SS316L cylindrical shells under pure torsional load: An experimental investigation", *Thin-Wall. Struct.*, **109**, 242-250.
Shi, D., Hu, X., Wang, J., Yu, H., Yang, X. and Huang, J. (2013), "Effect of notch on fatigue behaviour of a directionally solidified superalloy at high temperature", *Fatigue Fract. Eng. Mater. Struct.*, **36**(12), 1288-1297.
Varvani-Farahani, A., Kodric, T. and Ghahramani, A. (2005), "A method of fatigue life prediction in notched and un-notched components", *J. Mater. Process Tech.*, **169**(1), 94-102.
Wang, C. and Rose, L. (1998), "Transient and steady-state deformation at notch root under cyclic loading", *Mech. Mater.*, **30**(3), 229-241.
Zeng, Z. and Fatemi, A. (2001), "Elasto-plastic stress and strain behaviour at notch roots under monotonic and cyclic loadings", *J. Strain. Anal. Eng.*, **36**(3), 287-300.

CC